KSCE Journal of Civil Engineering (2021) 25(2):654-668
DOI 10.1007/s12205-020-5288-0

pISSN 1226-7988, eISSN 1976-3808
www.springer.com/12205

Surveying and Geo-Spatial Engineering

DPIM-Based InSAR Phase Unwrapping Model and a 3D Mining-Induced Surface Deformation Extracting Method: A Case of Huainan Mining Area

Chuang Jiang[a], **Lei Wang**[b], **Xuexiang Yu**[b], **Shenshen Chi**[b], **Tao Wei**[c], **and Xuelin Wang**[d]

[a]*School of Earth and Environment, Anhui University of Science and Technology, Huainan 232001, China*
[b]*School of Geodesy and Geomatics, Anhui University of Science and Technology, Huainan 232001, China*
[c]*Jiangsu Key Laboratory of Resources and Environmental Information Engineering, China University of Mining & Technology, Xuzhou 221116, China*
[d]*Nuclear and Roadway Engineering Group Company, Limited, Huzhou 313000, China*

ARTICLE HISTORY

Received 20 July 2020
Revised 1st 28 August 2020
Revised 2nd 13 September 2020
Accepted 4 October 2020
Published Online 17 December 2020

KEYWORDS

D-InSAR
Phase unwrapping
Mining subsidence
LOS deformation
Three-dimensional deformation

ABSTRACT

The mining subsidence in mining area could cause large-gradient deformation in a short period of time. When the deformation gradient exceeds the threshold value of the Differential Interferometry Synthetic Aperture Radar (D-InSAR) technology monitoring gradient, D-InSAR technology is likely to cause the failure of InSAR phase unwrapping algorithm. At this time, the InSAR technology is unable to monitor the 3D surface deformation. Aiming at these problems, an dynamic probability integral method (DPIM)-based InSAR phase unwrapping model and a method of extracting 3D surface deformation were proposed. The phase unwrapping model firstly used the empirical parameters of the probability integral of the mining face to predict the line of sight (LOS) direction deformation phase of the mining subsidence surface. Secondly, the phase of differential interferogram was unwrapped with the assist of the predicted LOS deformation phase under the constraint of DPIM, and the true LOS deformation phase was obtained, then the true LOS deformation phase transformed into LOS deformation. Finally, according to the geometric projection relationship between the LOS deformation and 3D deformation of mining subsidence surface, the probability integral prior model was brought into the equation of the geometric projection relationship. On the basis of relevant boundary conditions, the 3D surface deformation was extracted from the LOS direction deformation field of mining subsidence. The feasibility of the method was verified by the simulation experiment results. The differential interferogram of the subsidence basin was obtained by the differential interference processing of image data of Sentinel-1A on Nov. 16, 2017 and Dec. 10, 2017 of 1613 working face of Guqiao South Mine. By using the DPIM-based phase unwrapping model, the phase of differential interferogram was unwrapped and the 3D surface deformation during this period as well as the deformation extraction method were developed. The results showed that the maximum fitting error value of subsidence was 79 mm, about 8.33% of the maximum value of subsidence, and the fitting error of mean square of subsidence was ±33.5 mm. The results showed that the DPIM-based phase unwrapping model and the method of extracting 3D surface deformation proposed in this paper have certain engineering application values.

1. Introduction

When the underground coal resources are mined, the original mechanical equilibrium of the rock mass around the goaf will be destructed, which will cause rock strata movement and deformation, and even geological disasters. Under the influence of mining, the buildings, railways and cultivated lands will be deformed or damaged (Whittaker and Reddish, 1989; He et al., 1991; Kratzsch, 1983). Therefore,the research about the theory and method of mine deformation monitoring is of great scientific significance for early warning and prevention of geological disasters, and the safety of people in mining areas.

CORRESPONDENCE Lei Wang austwlei@163.com School of Geodesy and Geomatics, Anhui University of Science and Technology, Huainan 232001, China

Differential Interferometry Synthetic Aperture Radar (D-InSAR) has the advantages of all-weather, real-time, high-precision and large-area deformation field, so it can make up for the shortcomings of traditional leveling to monitor the 3D surface deformation. It has been successfully applied in various disaster monitoring (Massonnet et al., 1994; Sigurjón et al., 1999; Ferretti et al., 2000; Chaussard et al., 2013). It can provide important help for scholars to study mining subsidence (Carnec et al., 1996; Li et al., 2014; Fan et al., 2015a; Wang et al., 2018). However, due to the influence of radar return period and wavelength, there are two difficulties in using single line of sight (LOS) InSAR technology to monitor the 3D surface deformation. The first difficulty is when the gradient of surface deformation exceeds the detection capability of radar satellites, the large deformation gradient will be de-coherent, the phase unwrapping of differential interferogram in mining area will fail, and the true LOS deformation cannot be obtained (Zebker and Villasenor, 1992). The second difficulty is that the LOS deformation is essentially the sum of the 3D surface deformation along the LOS projection. It is very hard to get 3D surface deformation based on the LOS deformation value obtained by InSAR technology (Samsonov et al., 2013; He et al., 2015; Yang et al., 2018).

For the first difficulty, many scholars started from the technical direction and used offset-tracking technology to monitor the large-gradient deformation in the subsidence of coal mining (Zhao et al., 2013; Fan et al., 2015b; Huang et al., 2016). Yang et al. (2017a) used offset-tracking technology combined with genetic algorithm to further expand the application of large-gradient mining subsidence and deformation monitoring method (Yang et al., 2017a). The above research shows that offset tracking technology has certain effects on monitoring large-gradient deformation. However, the monitoring accuracy is generally only 1/10 – 1/20 of pixel resolution (Michel et al., 1999; Zhu et al., 2019). In addition, the intensity information will disappear and intensity-based offset tracking technology will fail when there is water accumulation in mining subsidence movement and deformation basin. Diao et al. (2018) used the phase unwrapping method and creatively proposed the phase unwrapping method based on the prediction model of the probability integral method, and a good unwrapping strategy was given (Diao et al., 2018). By this method, the LOS deformation phase and wrapped phase were predicted firstly by using the probability integral parameters under the similar geological and mining conditions. Secondly, the differential interference phase of InSAR and wrapped phase were subtracted, and phase unwrapping of the subtracted values was conducted. Then, the real LOS deformation phase of the surface was obtained by adding the unwrapping phase and the predicted phase. Finally, the LOS deformation phase was transformed to LOS deformation. This method reduces the difficulty of phase unwrapping of differential interferogram under large-gradient deformation and solves the problem of monitoring large-gradient deformation to a certain extent. However, the dynamic process of mining subsidence is unavailable by using a static probability integral model. Additionally, it takes the LOS deformation as the subsidence value, and does not consider the essence of movement and deformation, which is the sum of the subsidence and horizontal movement of the target point along the LOS projection, so it is unable to obtain the real surface LOS deformation.

For the second difficulty, Yang et al. (2016) proposed the "probability integral model + monorail D-InSAR prediction" method on the basis of the surface LOS deformation of mining subsidence (Yang et al., 2016). It firstly used the functional relationship between subsidence and horizontal movement in the probability integral model to represent the *NS* and *EW* horizontal movement as a function of subsidence. Then, the real observation equation was established by using the geometric relationship between LOS deformation and the 3D surface deformation. The parameters in the probability integral model were solved by using the observation equation. Finally, the parameters were brought back to the probability integral model to realize InSAR monitoring of 3D surface deformation. Li et al. (2014) and Wang et al. (2019) proposed the "probability integral model + D-InSAR observation" method based on the LOS deformation (Li et al., 2014; Wang et al., 2019). It is based on the geometric projection relationship between the LOS deformation and 3D surface deformation, and combines prior model of mining subsidence. Under the boundary conditions that the horizontal movement in last row and the last row of pixels was 0 in the LOS deformation field, the 3D surface deformation was extracted from the LOS deformation. Literature research shows that the premise of successful application of the above two kinds of 3D deformation monitoring methods (PIM+D-InSAR prediction method and PIM+D-InSAR observation method) is to obtain the LOS direction deformation of mining subsidence surface. Therefore, it is very important to obtain the deformation field of LOS deformation for 3D surface deformation monitoring. However, due to the limitations of InSAR monitoring gradient, the interference conditions, the baseline length of time and space, the LOS deformation are not easy to obtain.

In view of the shortcomings of only using LOS InSAR technology in monitoring 3D surface deformation caused by mining subsidence, this paper will develop a DPIM-based phase unwrapping model of InSAR and a method of extracting 3D deformation. Based on the ideas of literature Diao et al. (2018) Li et al. (2014) and Wang et al. (2019), this method will take the dynamically predict model of probability integral method as the constraint conditions. Firstly, the 3D surface deformation will be predicted during two periods. Secondly, the LOS deformation in two periods will be predicted based on the geometric projection relationships between subsidence, horizontal movement and LOS deformation of the target point. According to the relationship between the value and phase of LOS deformation, the winding phase of LOS deformation will be obtained. Then, the predicted winding phase will be used to assist the phase unwrapping of the interference phase in two periods, and the real LOS deformation value of any pixel on the surface could be obtained. Finally, on the basis of the real LOS deformation field, according to the geometric projection relationship between the LOS deformation

of D-InSAR and the subsidence, the horizontal movement in NS and EW directions, as well as the prior model of mining subsidence, the 3D surface deformation will be extracted from the LOS deformation under the boundary condition that the horizontal movement of the first row and the first row of pixels is 0 in the LOS deformation field.

Based on dynamic surface movement and deformation mechanism and geometry of imaging radar, this paper will discuss a DPIM-based phase unwrapping model and a method of extracting 3D surface deformation. Then the feasibility study will be carried out through simulation experiment. Finally, the model will be applied to the monitoring of the 3D surface deformation between Nov.16, 2017 and Dec.22, 2017 in the 1613 working face of Guqiao Coal Mine in Huainan mining area.

2. Methodology

2.1 A DPIM-Based Phase Unwrapping Model

According to the phase unwrapping theory, when the absolute value of the phase difference between adjacent pixels is less than 2π, continuous phase difference values can be used to achieve phase unwrapping. However, in the differential interferogram of SAR image in mining area, when the spatial incoherence occurs and the ground deformation gradient exceeds the detection ability of radar satellite, the large deformation gradient will become incoherent and the phase unwrapping will fail. In response to the above problems, Diao et al. (2018) firstly proposed the phase unwrapping method based on the prediction model of the probability integral method by studying the mechanism of horizontal coal seam movement and deformation (Diao et al., 2018). On the basis of Diao method, this paper proposes to build an InSAR phase unwrapping model suitable for horizontal and inclined seam mining subsidence monitoring based on the mining subsidence law in inclined coal seams.

According to the dynamic prediction principle of the probability integral method, the subsidence value of the surface point $A(x, y)$ after the Ti time of coal seam mining can be expressed as

$$W_{T_i}(x,y,P_{T_i}) = \sum_{T_i=1}^{T_i} \frac{1}{W_0}(W(x)-W(x-l_{T_i}))* (W(y)-W(y-D_i))*f(T_i), \tag{1}$$

$$W_0 = m*q*cos\alpha, \tag{2}$$

$$W(k) = \frac{W_0}{2}\left[erf\left(\frac{\sqrt{\pi}*tan\beta}{H_0}k\right)+1\right]. \tag{3}$$

After mining, the value of NS horizontal movement and EW horizontal movement of surface point $A(x, y)$ after T_i time can be expressed as

$$U_{N_{Ti}} = U_{T_i}(x,y,P_{T_i},\varphi_N)+\Delta Uy_{T_i}'*\cos\varphi_N, \tag{4}$$

$$U_{E_{Ti}} = U_{T_i}(x,y,P_{T_i},\varphi_E)+\Delta Uy_{T_i}'*\sin\varphi_E, \tag{5}$$

$$U_{T_i}(x,y,P_{T_i},\varphi) = b_{T_i}*r_{T_i}*\left(\frac{\partial W_{T_i}(x,y)}{\partial x}\cos\varphi+\frac{\partial W_{T_i}(x,y)}{\partial y}\sin\varphi\right), \tag{6}$$

$$\Delta Uy_{T_i}' = W_{T_i}(x,y,P_{T_i})\cdot\cot\theta, \tag{7}$$

$$f(T_i) = 1-e^{-cT_i}. \tag{8}$$

The meaning of each parameter in the above equations is

P_{T_i} — The predicted parameters of PIM model of the working face at T_i time

$$P_{T_i} = [q_{Ti}\quad Tan\beta\quad b\quad \theta_0\quad S_1\quad S_2\quad S_3\quad S_4\quad c]$$

b – Horizontal movement factor
D_1 – The length of dip of the working face
H_0 – Mining depth
l_{T_i} – Mining length of strike in T_i time
m – Coal seam thickness
r – The main influence radius
$tan\beta$ – The tangent of main influence angle
U – The horizontal movement value of the surface point $A(x, y)$
W – The subsidence value of the surface point $A(x, y)$
(x, y) – The plane coordinate of any point on the surface
δ – Coal seam dip angle
φ_{NS} – The included angle of the strike direction of the working face turning counterclockwise to the north direction
φ_{EW} – The included angle of the strike direction of the working face turning counterclockwise to the east direction
θ_0 – The greatest subsidence angle

According to the geometric relationship between LOS deformation value and the 3D deformation of the surface, the LOS value of the surface point A (x, y) after the T_i time of coal seam mining can be expressed as

$$LOS_{T_i}^j = -U_{SN_{Ti}}\sin\theta_j\cos\left(\alpha_j-\frac{3}{2}-\pi\right)- U_{EW_{Ti}}\sin\theta_j\sin\left(\alpha_j-\frac{3}{2}\pi\right)+W_{T_i}\cos\theta_j. \tag{9}$$

The meaning of each parameter in Eq. (9) is

θ_j – The incident angle of line of sight of satellite corresponding to the surface point A
δ_j – The azimuth angle of flight direction of satellite corresponding to the surface point A

It is known that in the dynamic process of the mining of the whole working face, the change of probability integral parameter q is large, and the change of other parameters is small. Therefore, the following assumptions are given. When the underground coal mining is full mining, $q_{T_i} = q_{T_{i-1}}$; When the mining is unsufficient, $q_{T_i} \neq q_{T_{i-1}}$, $q_{T_i} = q_{T_{i-1}} + \Delta q$, and the other probability integral parameters are considered unchanged, q is replaced by Boltzmann function Yang et al. (2017b).

$$q_{T_i} = q\left[A_2+\frac{A_1-A_2}{1+e^{(l_{T_i}/1.1H-A_3)/A_4}}\right] \tag{10}$$

The meaning of each parameter in Eq. (10) is as follows: A_1, A_2, A_3 and A_4 are Boltzmann constants. In Huainan mining area, $A_1 = 0$, $A_2 = 1$, A_3 and A_4 are in the interval (0.1, 1).

The deformation value of the differential interference LOS for T_i and T_{i-1} time period of the pixel j representing the surface point $A(x, y)$ after mining can be expressed as

$$\Delta LOS^{j}_{T_{i-1},T_i} = LOS^{j}_{T_i} - LOS^{j}_{T_{i-1}}. \tag{11}$$

According to the principle of D-InSAR technology, the relationship between the LOS deformation value and the deformation phase in any T_i, T_{i-1} period of the pixel j can be expressed as follows:

$$\phi^{j}_{defo} = -\frac{4\pi}{\lambda}\Delta LOS^{j_{defo}}_{T_{i-1},T}, \tag{12}$$

$$\phi^{j}_{defo} = \varphi^{j}_{defo} + k^{j}_{defo} \times 2\pi, \tag{13}$$

where λ is the radar incident wavelength, ϕ^{j}_{defo} is the actual interference deformation phase of pixel j representing the surface point A (x, y), $\Delta LOS^{j_{defo}}_{T_{i-1},T}$ is the actual LOS deformation, ϕ^{j}_{defo} is the actual interference winding phase, and k^{j}_{defo} is the integer ambiguities.

Similarly, the relationship between the predicted value of LOS deformation and the predicted phase of deformation of the pixel j representing the surface point A (x, y) can be expressed as

$$\phi^{j}_{pre} = -\frac{4\pi}{\lambda}\Delta LOS^{j_{Pre}}_{T_{i-1},T_i}, \tag{14}$$

$$\phi^{j}_{pre} = \varphi^{j}_{pre} + k^{j}_{pre} \times 2\pi, \tag{15}$$

where ϕ^{j}_{pre} is the predicted value of interference deformation phase of pixel j representing the surface point A (x, y), $\Delta LOS^{j_{Pre}}_{T_{i-1},T_i}$ is the predicted LOS deformation, ϕ^{j}_{pre} is the predicted interference winding phase, and k^{j}_{pre} is the integer ambiguities.

Therefore, after removing the predicted deformation phase from the actual deformation phase, the winding phase of the residual phase and the residual phase of the differential interferogram are as follows

$$\phi^{j}_{defo} - \phi^{j}_{pre} = (\varphi^{j}_{defo} - \varphi^{j}_{pre}) + (k^{j}_{defo} - k^{j}_{pre}) \times 2\pi = \phi^{j}_{Rp}, \tag{16}$$

$$\phi_{Rp}{}^{j} = \phi_{Rp}{}^{j} + (k^{j}_{defo} - k^{j}_{pre} + m^{j}) \times 2\pi, \tag{17}$$

where $\phi_{Rp}{}^{j}$ is the residual phase of the differential interferogram of pixel j representing the surface point A (x, y), $\varphi_{Rp}{}^{j} = mod[(\varphi^{j}_{defo} - \varphi^{j}_{pre}) + \pi, 2\pi] - \pi$ is the winding phase of $\phi_{Rp}{}^{j}$, and $(k^{j}_{defo} - k^{j}_{pre} + m^{j})$ is the integer ambiguities of $\phi_{Rp}{}^{j}$ of the pixel j of the surface point A (x, y).

At this time, since the difference between the adjacent pixels of the residual phase $\phi_{Rp}{}^{j}$ is small, the difficulty of phase unwrapping is reduced. Suppose that the phase unwrapping of the winding phase $\phi_{Rp}{}^{j}$ of the residual phase in the differential interferogram is $\phi_{Rp}{}^{j}$, according to Eq. (16), the true deformation phase of the surface can be expressed as

$$\phi^{j}_{defo} = \phi_{Rp}{}^{j} + \phi^{j}_{pre}. \tag{18}$$

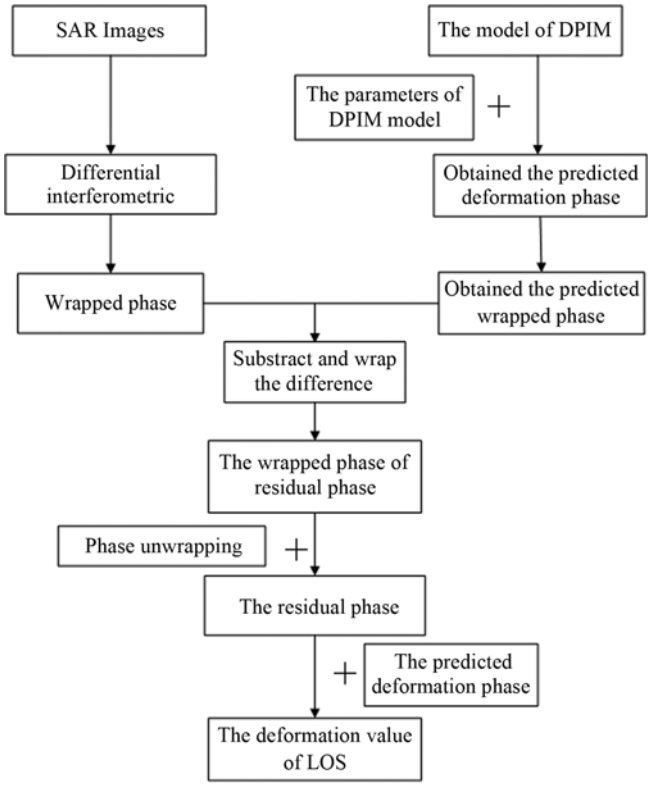

Fig. 1. The Flow Chart of the InSAR DPIM-Based Phase Unwrapping Model

Finally, according to the principle of D-InSAR technology, the deformation phase of the pixel j representing the surface point A (x, y) can be converted into the LOS deformation value by Eq. (12):

$$\Delta LOS^{j}_{T_{i-1},T_i} = -\frac{\lambda}{4\pi}\phi^{j}_{defo}. \tag{19}$$

The flow chart of the InSAR DPIM-based phase unwrapping model is shown in Fig. 1.

2.2 InSAR DPIM-Based Phase Unwrapping Model and a Method of Extracting 3D Surface Deformation

According to the mining subsidence principle and the literature Wu et al. (1998), Wang et al. (2019) and Li et al. (2014), the relationship between the NS horizontal movement of U_{SN} and the EW horizontal movement of U_{EW} and the subsidence W at any point on the mining surface of inclined coal seam is as follows:

$$U^{NS}_{ij} = b \cdot r \cdot \left(\frac{W_{i-1,j} - W_{i,j}}{\Delta x}\right) + W_{ij} \cdot \cot\theta \cdot \cos\varphi, \tag{20}$$

$$U^{EW}_{ij} = b \cdot r \cdot \left(\frac{W_{i,j-1} - W_{i,j}}{\Delta y}\right) + W_{ij} \cdot \cot\theta \cdot \sin\varphi. \tag{21}$$

In Eqs. (20) and (21), φ is the azimuth angle of coal seam inclination; r is the main effecting radius ($r = H / \tan\beta$); Δx is the resolution in the NS direction of the image and Δy is the

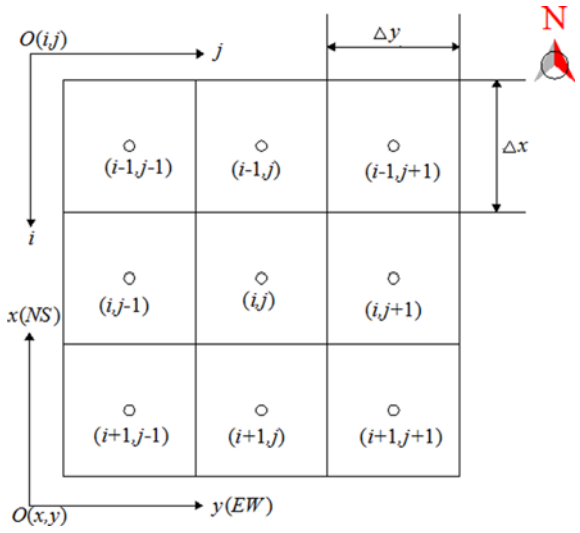

Fig. 2. Arrangement of Adjacent Pixels in SAR Images

resolution in the EW direction.

It can be seen from Eq. (9) that for the LOS deformation L_{ij} and subsidence W_{ij}, *NS* horizontal movement U_{ij}^{NS} and *EW* horizontal movement U_{ij}^{EW} monitored by D-InSAR of any pixel, there are the following projection relations:

$$L_{ij} = -U_{ij}^{NS}\sin\phi_{ij}\cos\left(\alpha_{ij}-\frac{3}{2}\pi\right)-U_{ij}^{EW}\sin\phi_{ij}\sin\left(\alpha_{ij}-\frac{3}{2}\pi\right)+W_{ij}\cos\phi_{ij}\,. \tag{22}$$

The simultaneous Eqs. (20), (21) and (22) are as follows:

$$L_{ij} = [C_1(i,j)\ C_2(i,j)\ C_3(i,j)]\begin{bmatrix} W_{i-1,j} \\ W_{i,j-1} \\ W_{i,j} \end{bmatrix}, \quad (i=1,2,\ldots,n, j=1,2,\ldots,m) \tag{23}$$

It can be seen from Eq. (23) that if we want to get the subsidence value W_{ij} of any pixel $A(i, j)$, we must firstly get the subsidence values $W_{i-1,j}$ and $W_{i,j-1}$ of its adjacent pixels $A(i–1, j)$ and $A(i, j–1)$. Generally speaking, the boundary of mining subsidence moving basin is mainly subsidence. Therefore, it is assumed that the horizontal movement value of mining subsidence basin boundary is zero. The following boundary conditions can be given for Eq. (23):

$$\begin{aligned} U_{ij}^{NS} &= 0 \quad (i=1; j=1,2,\ldots,n), \\ U_{ij}^{EW} &= 0 \quad (i=1,2,\ldots,m; j=1). \end{aligned} \tag{24}$$

At this time, the boundary part of Eq. (23) is converted into Eq. (24), that is

$$\begin{cases} L_{1j} = W_{1j}\cos\phi_{1j} = C4(1,j)*W_{1j} & (j=1,2,\ldots,n) \\ L_{1j} = W_{1j}\cos\phi_{i1} = C4(i,1)*W_{i1} & (i=1,2,\ldots,m). \end{cases} \tag{25}$$

The simultaneous Eqs. (23) and (25) are as follows:

$$L_{nm\times 1} = B_{mn\times mn}\cdot W_{mn\times 1}\,. \tag{26}$$

In Eq. (26),

$$L = \begin{bmatrix} L_{11} \\ L_{12} \\ \vdots \\ L_{1m} \\ \vdots \\ L_{n1} \\ L_{n2} \\ \vdots \\ L_{nm} \end{bmatrix},\ W' = \begin{bmatrix} W_{11} \\ W_{12} \\ \vdots \\ W_{1m} \\ \vdots \\ W_{n1} \\ W_{n2} \\ \vdots \\ W_{nm} \end{bmatrix},\ B_{mn\times mn} = \begin{bmatrix} B_a & & & & \\ B_2 & B_2' & & & \\ & B_3 & B_3' & & \\ & & \ddots & & \\ & & & B_{m-1} & B_{m-1}' \\ & & & & B_m \quad B_m' \end{bmatrix}$$

$$B_a = \begin{bmatrix} C4(1,1) & & & \\ & C4(1,2) & & \\ & & \ddots & \\ & & & C4(1,n) \end{bmatrix}_{n\times n} \qquad B_i = \begin{bmatrix} 0 & & & \\ & C4(i,2) & & \\ & & \ddots & \\ & & & C1(i,n) \end{bmatrix}_{n\times n}$$

$$B_i' = \begin{bmatrix} C4(i,1) & & & & \\ & C2(i,2) & C3(i,2) & & \\ & & \ddots & & \\ & & C2(i,n-1) & C3(i,n-1) & \\ & & & C2(i,n) & C3(i,n) \end{bmatrix}_{n\times n}$$

For the solution of Eq. (26), it can be solved by the back generation method based on the given boundary conditions. The specific steps are as follows. Firstly, according to the boundary conditions, the first row and the first column of pixels in the entire subsidence field $W(n, m)$ are calculated. On this basis, the subsidence values of the second row were calculated by bringing the subsidence values of the first row and first column into Eq. (26). By analogy, until the subsidence values of the n-th row are

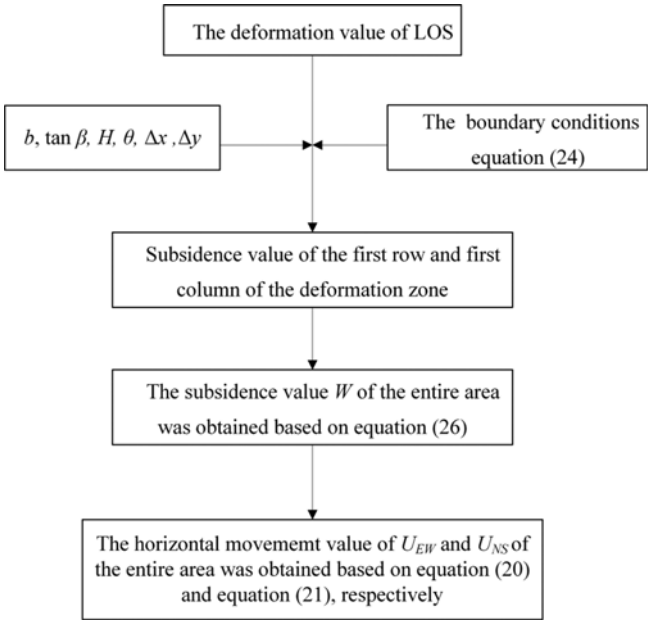

Fig. 3. The Flow Chart of the Method of Extracting 3D Surface Deformation

calculated, the subsidence field of the surface moving and deformation basin can be obtained.

Then, on the basis of the subsidence field of the whole moving and deformation basin, according to the Eqs. (20) and (21), we can calculate the NS horizontal movement U_{NS} and EW horizontal movement U_{EW} of A (x, y) pixel representing any point on the surface. Thus, the mining-induced 3D deformation can be obtained successfully.

The flowchart of the process presented in Section 2.2 as Fig. 3:

3. Simulated Experiment

3.1 Geological and Mining Conditions of Simulated Experiment

This paper simulates a mining face based on the mining conditions of Huainan mining area. The parameters of the probability integral method of the simulated working face are as follows: subsidence coefficient q = 0.9, horizontal movement factor b = 0.2, the main tangent of main influence angle $Tan\beta$ = 2.3, the greatest subsidence angle θ_0 = 85°, and the offset inflection point

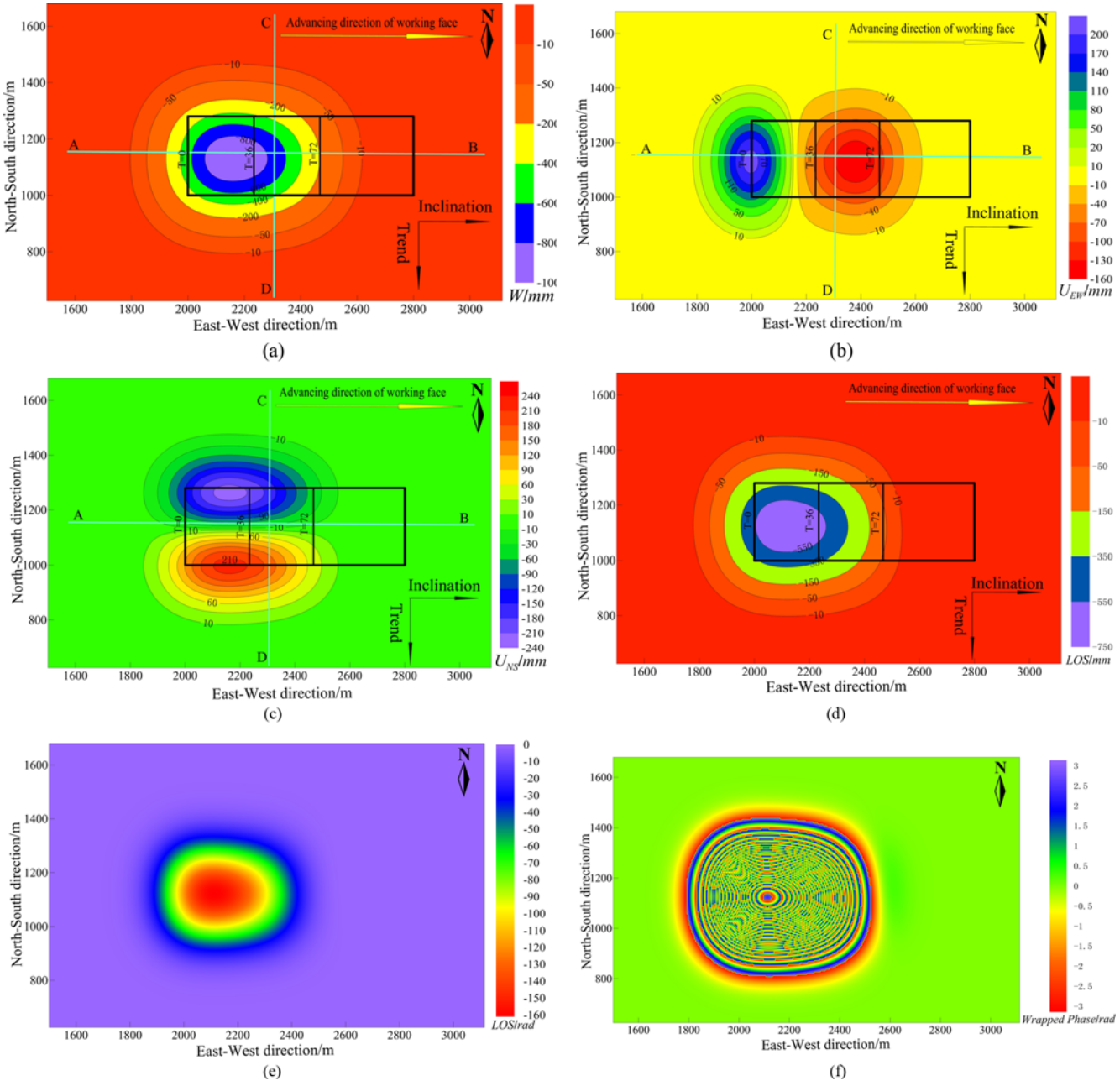

Fig. 4. Surface Deformation: (a) W between the 36th Day and 72nd Day, (b) U_{EW} between the 36th Day and 72nd Day, (c) U_{NS} between the 36th Day and 72nd Day, (d) LOS between the 36th Day and 72nd Day, (e) Deformation Phase of LOS, (f) Wrapped Phase of LOS

$S_1 = S_2 = S_3 = S_4 = 10$ m. The geological and mining conditions are as follows: coal seam dip angle $\delta = 0°$, coal seam thickness $m = 3$ m, mining depth $H_0 = 500$ m, the average mining velocity $v = 6.5$ m/d, azimuth of dip is 180°, time function of Knothe Guo et al. (2020) in Eq. (8) $c = 0.0296$, the Boltzmann constants in Eq. (10) $A_3 = 0.745$, $A_4 = 0.184$, the size of the working face along the dip is $D = 280$ m, and the size of the working face along the strike is $D_3 = 800$ m. Since the size of the working face meets the conditions of $D/H = 0.56 < 1.2 - 1.4$ and $D_3/H = 1.6 > 1.2 - 1.4$, the mining is not suffient. The planar graph of the simulated working is shown in Fig. 4(a), where AB and CD are the strike line and the dip line, respectively. The monitoring points are arranged on AB and CD at 10m intervals.

3.2 The Simulated Experiment of the DPIM-Based Phase Unwrapping Model

The surface above the working face was divided into a grid with an interval of 5 m along the north-south and east-west directions. The grid was used to simulate the SAR image with a resolution of 5 m (The resolution of azimuth and range direction is 5 m × 5 m). The parameters of the simulated satellite data are as follows: the return visit period of the satellite radar is 12 days, the incident angle of line of sight of satellite radar $\theta = 44.494°$, and the wavelength of satellite radar $\lambda = 56$ mm, and the azimuth angle of flight direction of satellite $\alpha = 350.596°$. Based on the simulated geological and mining conditions in Section 3.1 and the theory in Section 2.1, we got the subsidence (W), horizontal movement in East-West direction (U_{EW}), horizontal movement in North-South direction (U_{NS}), LOS deformation, the LOS deformation phase and wrapped phaseof the mining area between $T_{i-1} = 36$ and $T_i = 72$. The results are as follows:

The goal of this section is to realize the phase unwrapping of the differential interference phase diagram in Fig. 4, and make the unwrapping phase closest to the actual deformation phase in Fig. 4(e). However, in the practical application of mining area, the probability integral parameters of working face can not be obtained accurately, and in the prediction method of surface movement and deformation due to mining subsidence, the probability integral parameters have a crucial influence on the accuracy of 3D deformation prediction. They also generally have an important relationship with geological and mining conditions such as the thickness of loose layers, mining height, depth and degree. On the basis, the paper adopted different parameters from the data of the simulated working face in section 3.1 (variation of each parameter is within 10%), the specific probability integral predicted parameter values are as follows:

In Section 2.1, the DPIM-based phase unwrapping model was derived in strict accordance with mathematical criteria. In practice, the winding phase of the interferogram is within interval $(-\pi, \pi)$. However, the subtraction of the winding phase of the two interference phase diagrams can get the phase in the interval $(-2\pi, 2\pi)$ rather than the winding phase in interval $(-\pi, \pi)$. Therefore, we consider winding the winding phase difference of the two interferograms obtained above, and on the basis of winding phase of winding phase difference of the two interferograms, the winding phase of winding phase difference of the two interferograms is unwrapped, and the residual phase of the phase difference of the two interferograms is obtained. In order to verify the feasibility of the above method to get the residual phase of the phase difference of the two interferograms, based on the simulation data and the probability integral parameters given in Table 1, this paper used Section 2.1 to establish the model and the relevant MATLAB program to carry out the phase unwrapping experiment. The winding phase of winding phase difference of the two interferograms is shown in Fig. 5.

Table 1. Probability Integral Parameters Used in PU-DPIM Model

q	b	$Tan\,\beta$	θ	S_1	S_2	S_3	S_4	c	A_3	A_4
0.81	1.82	1.80	84	5	5	5	5	0.027	0.70	0.174

It can be seen from Fig. 5 that the figure of winding phase of winding phase difference of the two interferograms is obviously clearer than that of the actual interference winding phase, and the fringe density is significantly lower than that of the actual interference winding phase diagram Fig. 4. f. On this basis, the phase unwrapping of the winding phase of winding phase

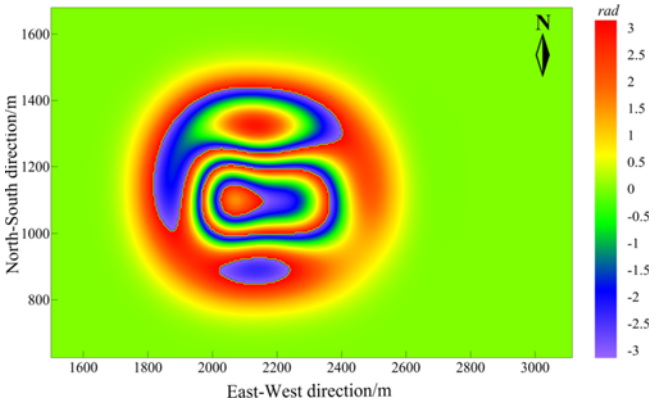

Fig. 5. The Winding Phase of Winding Phase Difference of the Two Interferograms

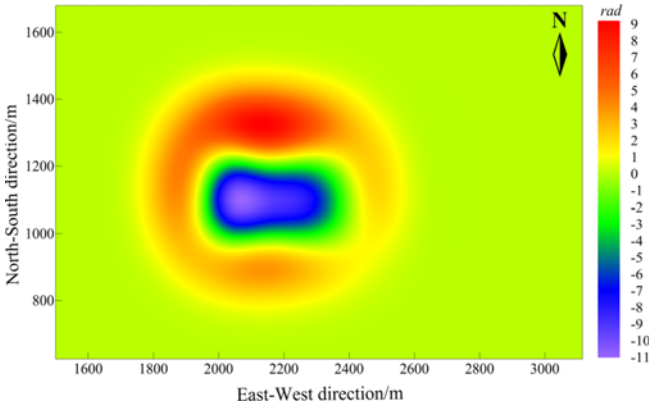

Fig. 6. The Residual Phase of the Phase Difference of the Two Interferograms

difference of the two interferograms in Fig. 5 was carried out, and the results are shown in Fig. 6 as follows:

The results showed that when the error of the probability integral parameter was within 10% of the actual probability integral parameter, the relative error between the residual phase of the phase difference of the two interferograms value $\phi_{Rp}^{\ j}$ and the actual residual phase through the DPIM-based phase unwrapping model is between -0.001 and 0.001 rad (converted to deformation error of 0.009 mm). The results show that the phase unwrapping model can achieve phase unwrapping of differential interference images without noise. Finally, based on the interference phase difference of the two interferograms

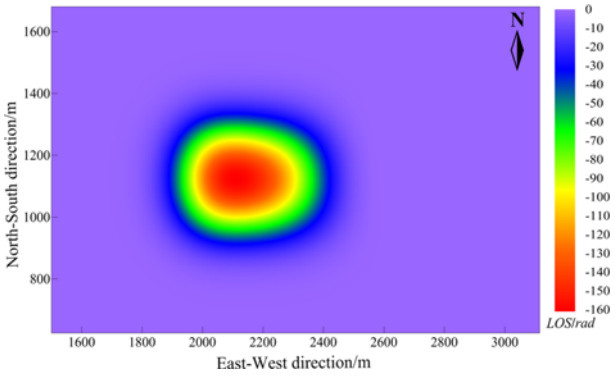

Fig. 7. LOS Deformation Phase Obtained by the Method in This Paper

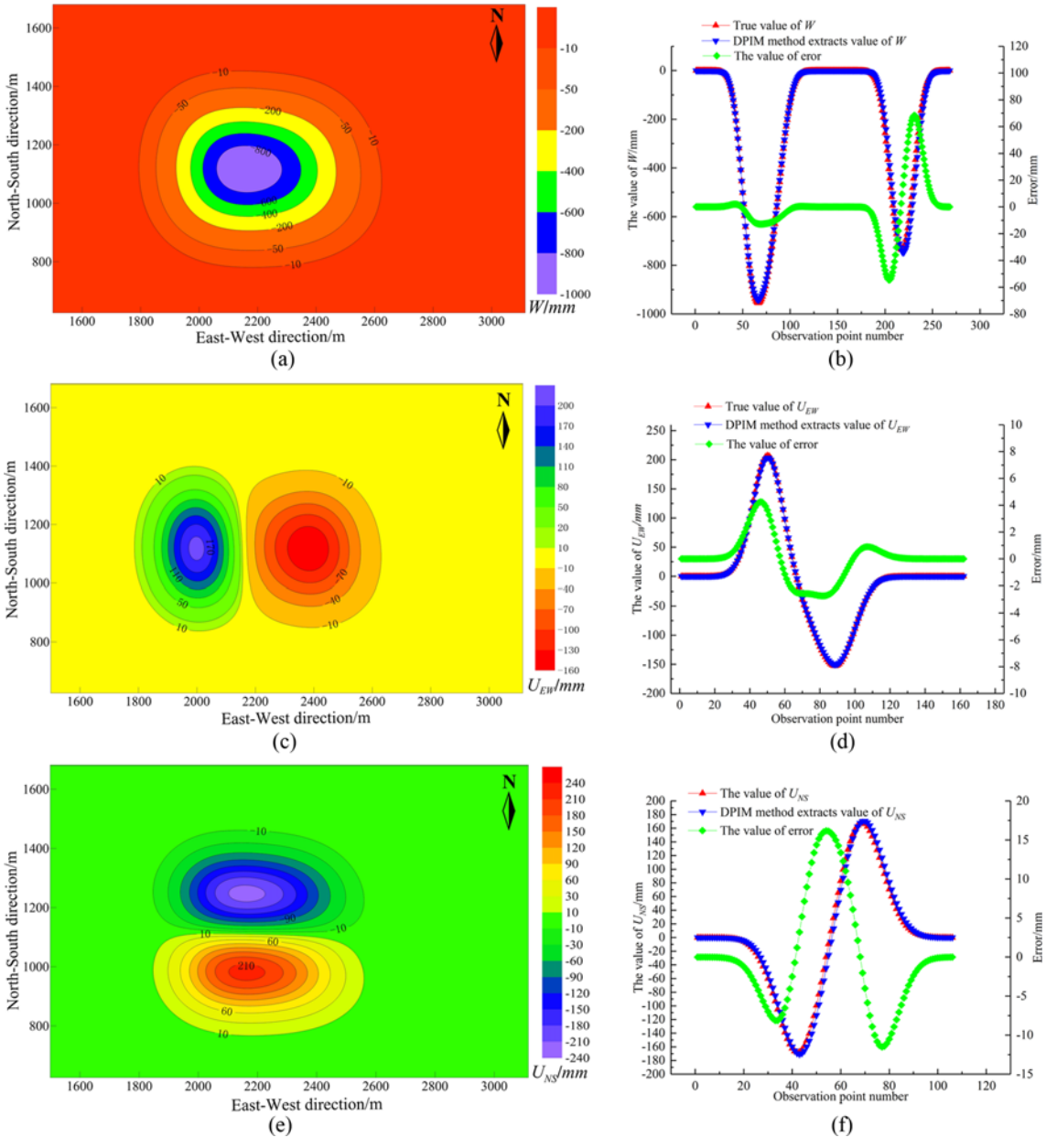

Fig. 8. 3D Surface Deformation Extracted by the Method in This Paper: (a) The Extracted W by This Paper Proposed Method, (b) Fitting of the W of Section AB and CD, (c) The Extracted U_{EW} by This Paper Proposed Method, (d) Fitting of the U_{EW} of Section AB, (e) The Extracted U_{NS} by This Paper Proposed Method, (h) Fitting of the U_{NS} of Section CD

obtained above and the predicted deformation phase, the actual surface deformation phase can be obtained by Eq. (18). The result is shown below:

3.3 The Simulated Experiment of Extracting Mining-Induced 3D Surface Deformation Based on InSAR DPIM-Based Phase Unwrapping Model

The surface LOS deformation phase data of mining subsidence can be obtained according to section 3.2, and the LOS deformation field can be obtained by Eq. (19). Based on the obtained D-InSAR LOS deformation field, the InSAR DPIM-based phase unwrapping model and the 3D surface deformation extracting method established in Section 2.3, the NS horizontal movement of U_{SN} and the EW horizontal movement of U_{EW} and the subsidence W in the simulated experimental area were extracted. The extracted surface movement and deformation fields are shown in Fig. 8.

In order to verify the correctness of the monitoring results of the method in this paper, the subsidence W, East-West horizontal movement U_{EW} and North-South horizontal movement U_{NS} of the observation points on the observation lines of AB and CD profiles in the simulated working face were extracted, respectively, and the relative errors were calculated. The absolute values of relative errors of W, U_{EW} and U_{NS} are shown in Figs. 8(b), 8(d) and 8(f), respectively.

It can be seen in Fig. 8 that the absolute error range of subsidence is - 54.58 mm – 68.37 mm, the absolute error range of U_{EW} of AB section is - 2.72 mm – 4.24 mm, and the absolute error range of U_{NS} of CD section is - 11.51 mm – 16.17 mm. At last, the RMS errors (RMSE) of the 3D deformation extracted from AB and CD sections were calculated, as shown in Table 2.

It can be seen that the RME errors of W and U_{EW} of AB section and U_{NS} of CD section are 14.01 mm, 1.21 mm and 3.85 mm, respectively. It shows that the InSAR DPIM-based phase unwrapping model and the 3D surface deformation extracting method have high accuracy in monitoring mining subsidence, and could meet the accuracy requirements of conventional technology to obtain the 3D deformation.

Table 2. RMS Errors of 3D Deformation

Direction	W	U_{EW} of AB section	U_{NS} of CD section
RMSES/mm	14.01	1.21	3.85

4. Engineering Application

4.1 General Situation of Geological and Mining Conditions and Satellite Data of the Experimental Area

The research object is 1613 working face of Guqiao South Mine in Huainan. It is located in Fengtai County, Anhui Province. Its geographical coordinates are 116° 26′ 15″ – 116° 37′ 00″ East longitude and 32° 43′ 47″ – 32° 52′ 30″ North latitude. The mining area is rich in coal resources, and is the largest mining mine in Asia. The 1613 working face started mining on March 36, 2017. Its geological and mining conditions are as follows: the coal seam dip angle δ = 3°, coal seam thickness m = 2.9 m, mining depth H_0 = 668 m, the average mining velocity v = 5.56 m/d, azimuth of dip is 21°, the size of the working face along the dip is D = 233 m, and the size of the working face along the strike is D_3 = 1,600 m. The geographical location and 1613 working face of Guqiao South Mine are shown in Fig. 9.

The radar image of the study area adopted the sentry 1A data with a resolution of 5 m × 20 m, and the radar data cover the whole study area. In this paper, two Sentinel-1A SAR images with a time baseline of 36 days from Nov. 16, 2017 (235d from mining time) to Dec. 22, 2018 (270d from mining time) were used. Sentinel-1A data radar wavelength λ = 56 mm, incidence angle Φ = 34.493°, and azimuth angle in the direction of satellite

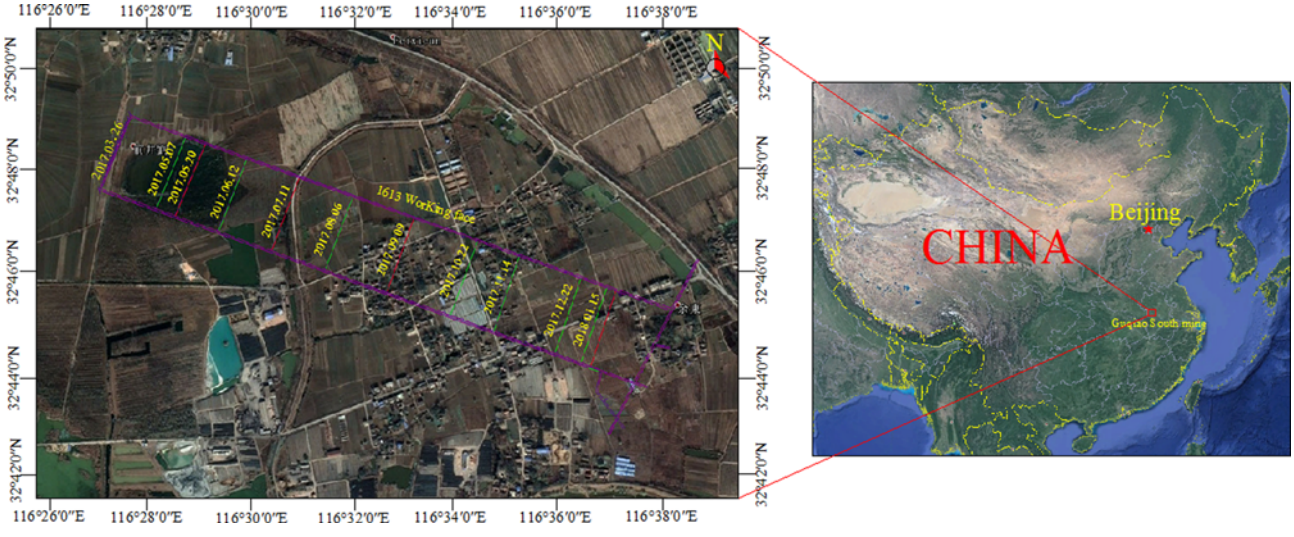

Fig. 9. The Location of the Working Face

line of sight $\alpha = 347.192°$.

4.2 Phase Unwrapping Experiment in the Study Area

The study area is 1613 working face of Guqiao South Mine in Huainan. According to the geological and mining conditions and empirical equation, the probability integral parameters of the working face are given in Table 3. The knote time function in Eq. (8) is c = 0.05, the Boltzmann constant in Eq. (10) is A_3 = 0.0.74375, A_4 = 0.016875. (parameters c, A_3 and A_4 were retrieved by given probability integral parameters and a small number of observation point data).

Firstly, based on the probability integral parameters in Table 3 and the geological and mining conditions of the Guqiao 1613 working face, the LOS deformation in the period of the mining time $T_{i-1} = 235$d and $T_i = 270$d was predicted. Secondly, the theory of Section 2.2 was used to predict the phase of surface LOS deformation and the predicted winding phase was obtained after winding. Then, D-InSAR was conducted for two scenes of Sentinel-1A SAR images by the SARscape software two-track differential technology to obtain the differential interference from Nov. 16, 2017 to Dec. 22, 2017, and Fig. 10 was obtained after geocoding the differential interference phase map. Finally, InSAR DPIM-based phase unwrapping model established in Section 2.1 and the minimum cost flow method were used to unwrap the phase diagram of differential interference between Nov. 16, 2017 and Dec. 22, 2017. The results of phase unwrapping by the minimum cost flow method are shown in Fig. 11, and the results by the method proposed in this paper are shown in Fig. 12.

Table 3. Probability Integral Parameters of 1613 Working Face

q	b	$Tan\ \beta$	θ	S_1	S_2	S_3	S_4
0.87	0.32	2.76	86.5	6.25	12.5	-4.7	21.8

It can be seen from Fig. 11 that due to the large fringe density in the interference phase diagram and the influence of noise, the minimum cost flow method cannot achieve the phase unwrapping of all pixels in the study area, and the maximum phase value is only 12.82 rad, which is completely inconsistent with the actual deformation phase. Fig. 12 shows that the maximum deformation phase obtained by the InSAR DPIM-based phase unwrapping model in this paper is 200 rad, and the deformation phase conforms to the mining subsidence law.

4.3 3D Deformation Monitoring Results and Accuracy Analysis

In order to obtain 3D surface deformation of mining subsidence, based on the LOS deformation in the mining surface in section 4.2, 3D deformation data were obtained by the method proposed in Section 2.3. The results are shown in Fig. 13. Secondly, according to the layout of the surface movement observation station in conventional coal mining, the subsidence values of 32

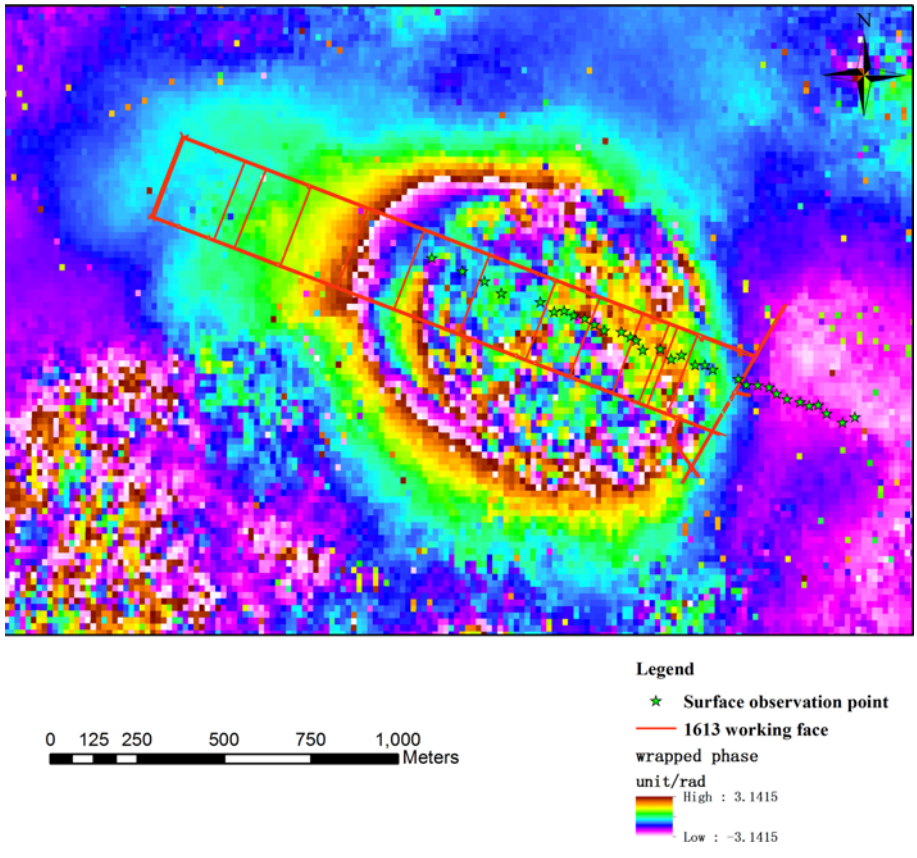

Fig. 10. Differential Interferometric Phase Image

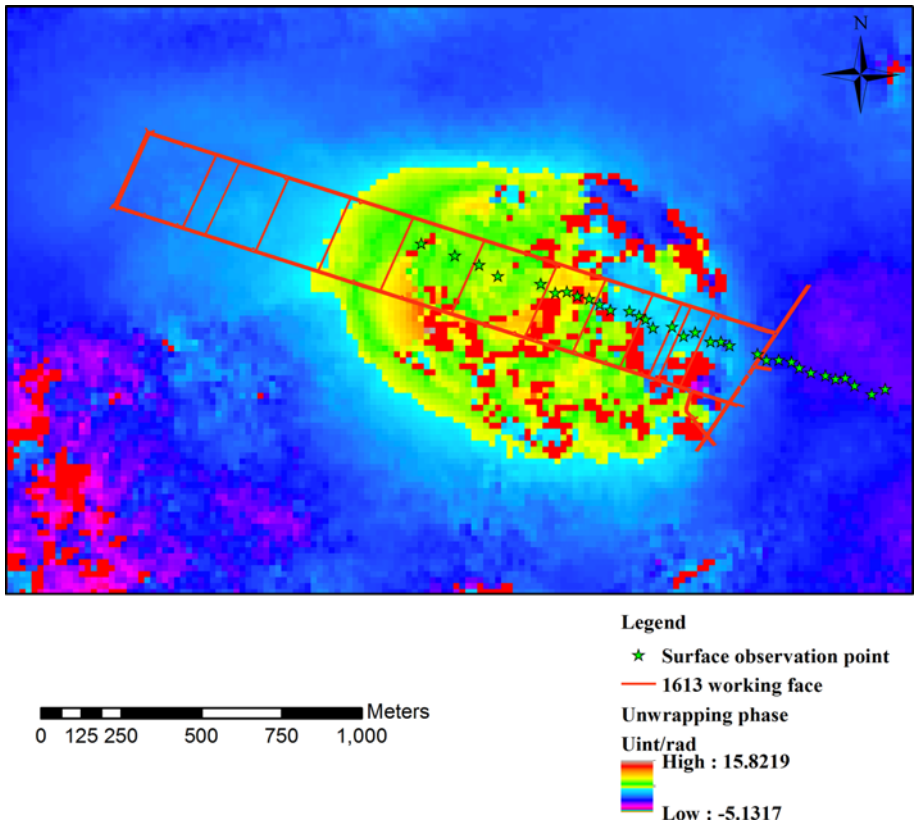

Fig. 11. Phase Unwrapping by MCF Method

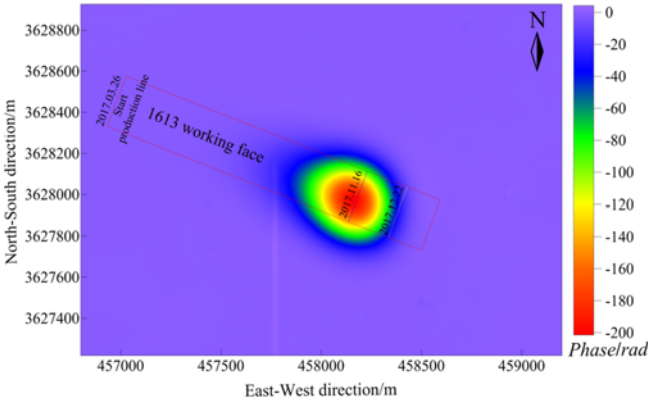

Fig. 12. The Results of Phase Unwrapping Based on DPIM-Based Phase Unwrapping Model

discrete pixel observation points in the strike section of the working face were taken and compared with the measured data for verification. The results are shown in Fig. 13(d).

In order to verify the accuracy of the InSAR DPIM-based phase unwrapping model and 3D surface deformation extracting method, the subsidence value extracted by this method in this paper was compared with the measured data. The results are shown in Fig. 13(d). The measured subsidence value curve and the extracted subsidence value curve are highly consistent, and the basin trend is basically the same. The fitting error of subsidence is 79 mm (8.33% of the maximum subsidence value), and the fitting error is ±33 mm (3.5% of the maximum subsidence value). The experimental results show that the InSAR DPIM-based phase unwrapping model and method of extracting 3D deformation of mining surface can extract 3D deformation of mining subsidence basin, and the research model has certain engineering application values.

5. Discussions

In the simulation experiment in Section 3.2, the probability integral parameters of the working face cannot be obtained accurately, however, they have a crucial influence on the prediction accuracy of the 3D surface deformation of mining subsidence. They generally have an important relationship with geological and mining conditions such as the thickness of loose layers, mining height, depth and degree. In the engineering application in the paper, under the similar geological and mining conditions, the probability integral parameters were given by empirical equations (the empirical values of the probability integral parameters of Guqiao mining area in Huainan were selected in the paper). Therefore, in order to study the influence of the probability integral parameters on the accuracy of the 3D surface deformation extracted by this method, the following four experimental schemes were designed: 1) The probability integral parameters $P = P–15\%·P$; 2) $P = P+15\%·P$; 3) $P = P–20\%·P$;

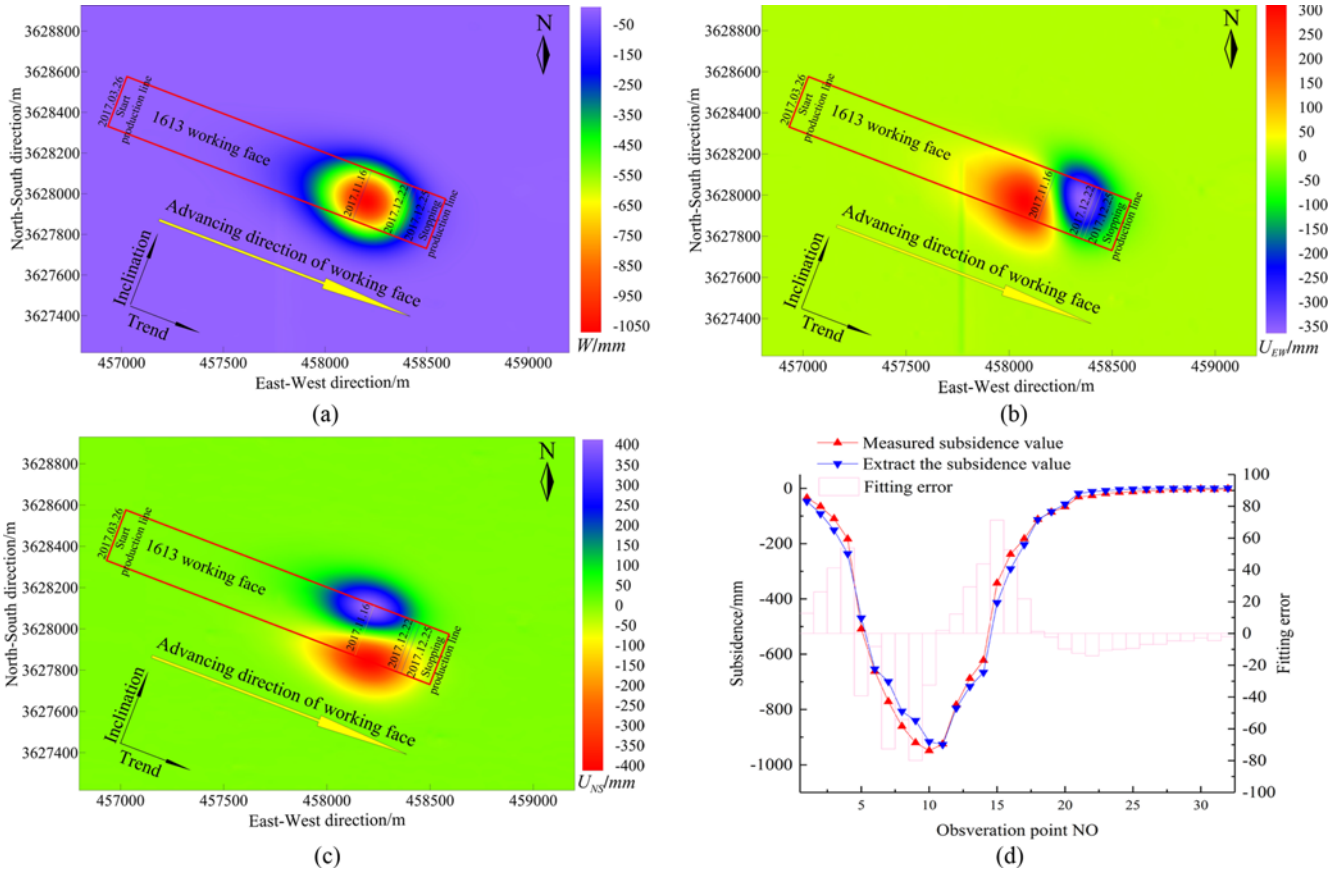

Fig. 13. 3D Deformation Values of the Surface in the Mining Area: (a) Surface Subsidence and Deformation, (b) EW Horizontal Movement and Deformation, (c) NS Horizontal Movement and Deformation, (d) Subsidence Comparison

Table 4. The Specific Probability Integral Parameters of the Four Experimental Design

Plan	q	b	Tan β	θ	S_1	S_2	S_3	S_4	c	A_3
Plan 1	0.765	0.17	1.7	83	8.5	8.5	8.5	8.5	0.0255	0.63325
Plan 2	1.035	0.23	2.3	86	11.5	11.5	11.5	11.5	0.0345	0.85675
Plan 3	0.72	0.16	1.6	87	8	8	8	8	0.024	0.596
Plan 4	1.08	0.24	2.4	88	12	12	12	12	0.036	0.894

and 4) $P = P+20\%\cdot P$. The specific probability integral parameters are shown in the Table 4 (the greatest subsidence angle θ_0 is generally between 83° and 89°).

Based on the D-InSAR simulated interference phase field in the mining area obtained by the simulation experiment in section 3.1, and the above four schemes, the DPIM-based phase unwrapping model established in Section 2.2 was used to unwrap the simulated interference phase firstly. Secondly, by the proposed model and method of extracting 3D surface deformation, the subsidence field W, the North-South horizontal movement USN and the East-West horizontal movement U_{EW} in the simulated experimental area were extracted. The subsidence and horizontal movement were extracted along the section lines AB and CD, respectively, and the maximum relative error and RMS error were calculated. The results are shown in Fig. 14 and Table 5.

It can be seen that after the probability integral parameters exceed 15%, the maximum relative error and RMS error of subsidence extracted by this method are 70.21 mm and 102.9 mm, respectively; the maximum relative error and RMS error of U_{EW} in profile AB are 5.80 mm and 2.18 mm, respectively; the maximum relative error and RMS error of U_{NS} in profile CD are 34.74 mm and 15.85 mm, respectively. At this time, the error of U_{NS} is larger than that of subsidence and U_{EW}. Based on the above analysis, without considering the LOS deformation error and the probability integral parameter error is selected within 15% of the actual probability integral parameter, the 3D deformation of the entire mining subsidence basin can be monitored effectively by using the method proposed in this paper.

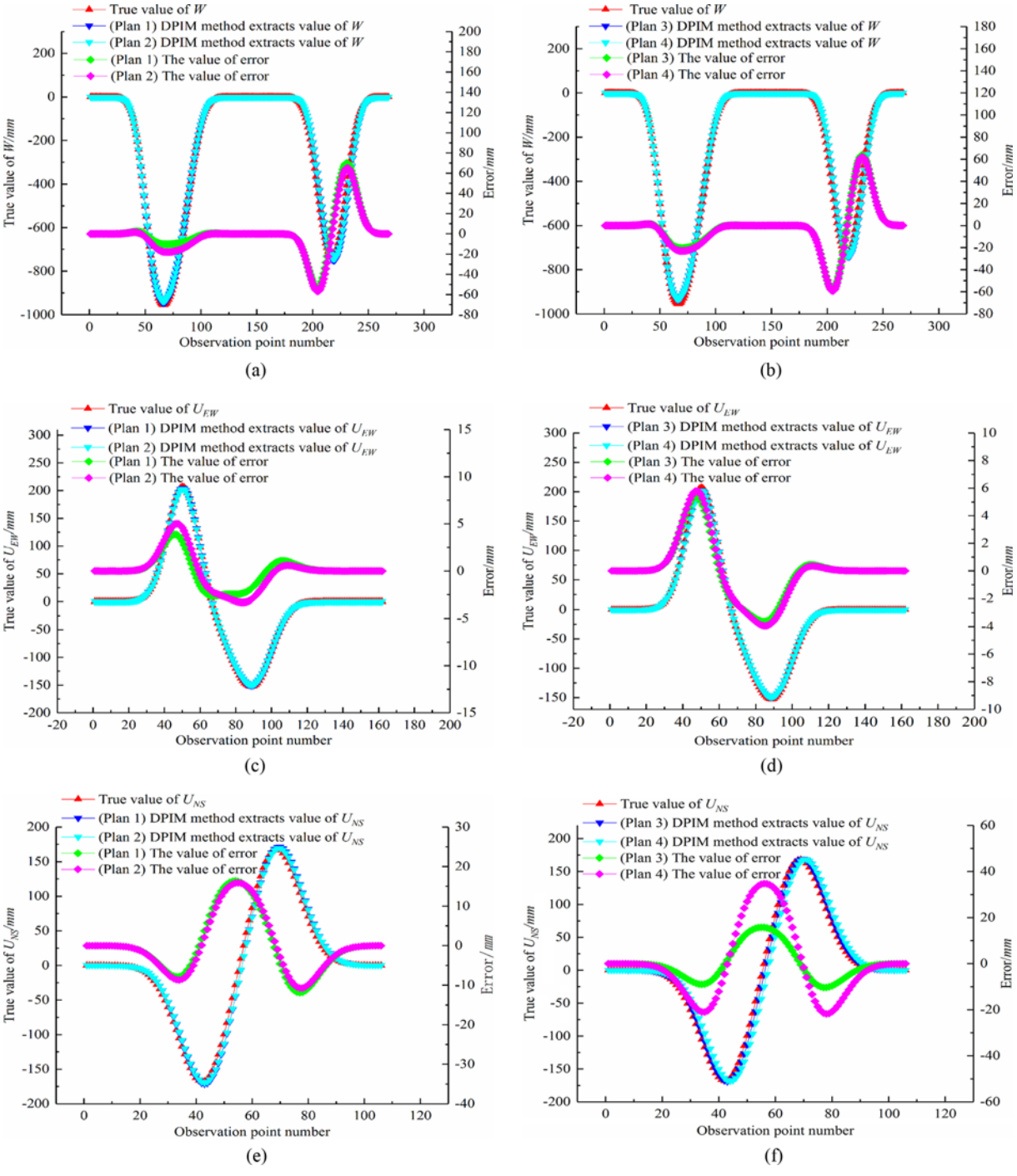

Fig. 14. 3D Deformation Extraction Profile: (a) Plan1 and Plan2 *W* Profile Map, (b) Plan3 and Plan4 *W* Profile Map, (c) Plan1 and Plan2 U_{EW} Profile Map, (d) Plan3 and Plan4 U_{EW} Profile Map, (e) Plan1 and Plan2 U_{NS} Profile Map, (f) Plan1 and Plan2 U_{NS} Profile Map

Table 5. Values of 3D Surface Deformation

Deformation	*W*		U_{EW}		U_{NS}	
Plan	Relative error/mm	RMSES/mm	Relative error/mm	RMSES/mm	Relative error/mm	RMSES/mm
Plan1	-53.52 – 69.99	20.63	-2.64 – 3.88	1.51	-11.91 – 16.35	7.46
Plan2	-56.78 – 65.17	20.72	-3.31 – 5.01	1.87	-10.72 – 15.88	7.23
Plan3	-57.93 – 63.60	20.87	-3.62 – 5.40	2.02	-10.34 – 15.75	7.18
Plan4	-59.07 – 62.04	21.06	-3.95 – 5.80	2.18	-21.78 – 34.74	15.85

6. Conclusions

1. Taking the dynamic prediction model of mining subsidence as the constraint condition, the LOS deformation phase given under DPIM constraint was used to assist the phase unwrapping of the differential interference phase diagram of the mining area, and the large-gradient deformation in D-InSAR LOS of mining subsidence was obtained. According to the geometric projection relationship between the LOS deformation of D-InSAR and the subsidence, the horizontal movement in NS and EW directions, and the prior model of mining subsidence and the geometric projection relationship, under the boundary condition that the horizontal movement in the first row and the first row of pixels was 0 in the LOS deformation field, the 3D surface deformation was extracted from the LOS deformation.
2. The DPIM-based phase unwrapping model and method of extracting 3D deformation of mining surface were verified by simulation experiments. The extracted absolute error range of subsidence was between -54.58 mm – 68.37 mm, and the fitting error was 20.60 mm; the absolute error range of UEW of AB section was between -2.72 mm – 4.24 mm, and the fitting error was 1.61 mm; The absolute error of UNS of the CD section was between -11.51 mm and 16.17 mm, and the fitting error is 7.37 mm. It shows that the method established in this paper has high accuracy in monitoring the 3D surface deformation, and could meet the accuracy requirements of the conventional technology to obtain the 3D deformation.
3. The engineering application results of 1613 working face show that the method proposed in this paper overcomes the defects of the conventional phase unwrapping methods in rapid surface deformation area, and can complete the recovery of the winding phase in dense areas with high fringes. The subsidence value extracted by this method in this paper was compared with the measured subsidence value of the working face strike profile. The results show that the measured subsidence value curve and the extracted subsidence value curve were highly consistent, and the basin trend was basically the same. The fitting error of subsidence was 79 mm (8.33% of the maximum subsidence value), and the fitting error was ±33 mm (3.5% of the maximum subsidence value). The experimental results show that the method propose in this paper can extract 3D deformation of mining subsidence basin.
4. When the mining area have the parameters of probability integral method of the first mining face (the probability integral parameter error is selected within 15% of the actual probability integral parameter). In this case, the method in this paper can be used to monitor the surface deformation caused by the mining of other working faces in the mining area.

Acknowledgments

The authors thank the European Space Agency (ESA) for providing the radar images data of Sentinel-1. The authors thanks to reviewers for spending a lot of time reviewing manuscripts.
The work was supported by the National Natural Science Foundation of China [Grant numbers 52074010, 41602357, 41474026, 51904008].

ORCID

Chuang Jiang https://orcid.org/0000-0002-0906-425X
Lei Wang https://orcid.org/0000-0001-8483-0471

References

Carnec C, Massonnet D, King C (1996) Two examples of the use of sar interferometry on displacement fields of small spatial extent. *Geophysical Research Letters* 23(24):3579-3582, DOI: 10.1029/96GL03042

Chaussard E, Amelung F, Abidin H, Hong SH (2013) Sinking cities in Indonesia: ALOS PALSAR detects rapid subsidence due to groundwater and gas extraction. *Remote Sensing of Environment* 128:150-161, DOI: 10.1016/j.rse.2012.10.015

Diao XP, Wu K, Xu YK, Zhou DW, Chen RL (2018) Prediction-based phase unwrapping for differential interferograms of coal mining areas using a stochastic medium model. *Remote Sensing Letters* 9(5):478-487, DOI: 10.1080/2150704X.2018.1441561

Fan HD, Cheng D, Deng KZ, Chen BQ, Zhu CG (2015a) Subsidence monitoring using D-InSAR and probability integral prediction modelling in deep mining areas. *Survey Review* 47(345):438-445, DOI: 10.1179/1752270614Y.0000000153

Fan HD, Gao XX, Yang JK, Deng KZ, Yang Y (2015b) Monitoring mining subsidence using a combination of phase-stacking and offset-tracking methods. *Remote Sensing* 7(7):9166-9183, DOI: 10.3390/rs70709166

Ferretti A, Rocca F, Prati C (2000) Nonlinear subsidence rate estimation using permanent scatterers in differential SAR interferometry. *IEEE Transactions on Geoscience and Remote Sensing* 38(5):2202-2212, DOI: 10.1109/36.868878

Guo XW, Yang XQ, Chai SW (2020) Optimization of the segmented Knothe function and its dynamic parameter calculation. *Rock and Soil Mechanics* 41(06):2091-2097+2109, DOI: 10.16285/j.rsm.2019.1567 (in Chinese)

He LM, Wu LX, Liu SJ, Wang Z, Su C, Liu SN (2015) Mapping two-dimensional deformation field time-series of large slope by coupling DInSAR-SBAS with MAI-SBAS. *Remote Sensing* 7(9):12440-12458, DOI: 10.3390/rs70912440

He GQ, Yang L, Ling GD, Jia FC, Hong D (1991) Mining subsidence science. China University of Mining and Technology Press, Xuzhou, China, 27-37

Huang JL, Deng KZ, Fan HD, Lei SG, Yan SY, Wang L (2017) An improved adaptive template size pixel-tracking method for monitoring large-gradient mining subsidence. *Journal of Sensors* 2017:1-11, DOI: 10.1155/2017/3059159

Huang JL, Deng KZ, Fan HD, Yan SY (2016) An improved pixel-tracking method for monitoring mining subsidence. *Remote Sensing Letters* 7(8):731-740, DOI: 10.1080/2150704X.2016.1183177

Kratzsch H (1983) Mining subsidence engineering. Springer-Verlag, Berlin, Germany

Li ZW, Yang ZF, Zhu JJ, Hu J, Wang YJ, Li PX, Chen GL (2014) Retrieving three-dimensional displacement fields of mining areas from a single InSAR pair. *Journal of Geodesy* 89(1)1:17-32, DOI: 10.1007/s00190-014-0757-1

Massonnet D, Feigl K, Rossi M, Adragna F (1994) Radar interferometric mapping of deformation in the year after the Landers earthquake. *Nature* 369(6477): 227-230, DOI: 10.1038/369227a0

Michel R, Avouacjp JP, Taboury J (1999) Measuring ground displacements from SAR amplitude images: Application to the landers earthquake. *Geophysical Research Letters* 26(7):875-878

Samsonov S, Oreye ND, Smets B (2013) Ground deformation associated with post-mining activity at the French–German border revealed by novel InSAR time series method. *International Journal of Applied Earth Observation and Geoinformation* 23:142-154, DOI: 10.1016/j.jag.2012.12.008

Sigurjón J, Zebker H, Cervelli P, Segall P, Garbeil H, Mouginis MP, Rowland S (1999) A shallow-dipping dike fed the 1995 flank eruption at Fernandina Volcano, Galápagos, observed by satellite radar interferometry. *Geophysical Research Letters* 26(8):1077-1080, DOI: 10.1029/1999gl900108

Wang L, Jiang C, Zhang XN, Zha JF (2019) Monitoring method of surface subsidence induced by inclined coal seam mining based on single line of sight D-InSAR. *Geomatics and Information Science of Wuhan University* 44(6):814-820, DOI: 10.13203/j.whugis20170300 (in Chinese)

Wang L, Zhang XN, Chi SS, Zha JF (2018) Parameter inversion model for mining subsidence prediction based on fusion of InSAR and GA. *Geomatics and Information Science of Wuhan University* 43(11): 1635-1641, DOI: 10.13203/j.whugis20170088 (in Chinese)

Whittaker BN, Reddish DJ (1989) Subsidence: Occurrence, prediction, and control. Elsevier, Amsterdam, The Netherlands, DOI: 10.1016/0148-9062(90)95372-8

Wu K, Ge JX, Wang LD, Zhou M (1998) Integration methods of mining subsidence prediction. China University of Mining and Technology Press, Xuzhou, China, 28-39

Yang ZF, Li ZW, Zhu JJ, Axel P, Yi HW, Hu J, Feng GC, Markus P (2017a) Retrieving 3-D large displacements of mining areas from a single amplitude pair of SAR using offset tracking. *Remote Sensing* 9(4):338, DOI: 10.3390/rs9040338

Yang ZF, Li ZW, Zhu JJ, Feng GC, Wang QJ, Hu J, Wang CC (2018) Deriving time-series three-dimensional displacements of mining areas from a single-geometry InSAR dataset. *Journal of Geodesy* 92: 529-544, DOI: 10.1007/s00190-017-1079-x

Yang ZF, Li ZW, Zhu JJ, Hu J, Wang YJ, Chen GL (2016) InSAR-based model parameter estimation of probability integral method and its application for predicting mining-induced horizontal and vertical displacements. *IEEE Transactions on Geoscience and Remote Sensing* 54(8):4818-4832, DOI: 10.1109/tgrs.2016.2551779

Yang ZF, Li ZW, Zhu JJ, Preusse A, Yi HW, Wang YJ, Papst M (2017b) An extension of the InSAR-based probability integral method and its application for predicting 3-D mining-induced displacements under different extraction conditions. *IEEE Transactions on Geoscience and Remote Sensing* 55(7):3835-3845

Zebker HA, Villasenor J (1992) Decorrelation in interferometric radar echoes. *IEEE Transactions on Geoscience and Remote Sensing* 30(5): 950-959, DOI: 10.1109/36.175330

Zhao CY, Lu Z, Zhang Q (2013) Time-series deformation monitoring over mining regions with SAR intensity-based offset measurements. *Remote Sensing Letters* 4(5):436-445, DOI: 10.1080/2150704X.2012.746482

Zhu JJ, Yang ZF, Li ZW (2019) Recent progress in retrieving and predicting mining-induced 3D displacements using InSAR. *Acta Geodaetica et Cartographica Sinica* 48(2):135-144, DOI: 10.11947/j.AGCS.2019.20180188 (in Chinese)